Chapter 6

Results

The details of the experiments performed have been outlined in the last chapter. In this chapter we give the techniques used for data reduction and also present the results. The first section describes the method used for obtaining the fusion excitation function and the barrier distribution while the second section gives the details for getting the quasi-elastic excitation function and the barrier distribution from them.

6.1 Fusion

The evaporation residues were detected at the focal plane of HIRA. The detected ER's form part of the total fusion cross section as HIRA has a limited acceptance in terms of energy, mass, charge state and angle. The total cross section is calculated after making appropriate correction for the efficiency of HIRA. The method employed to estimate the efficiency is given below.

Estimation of Detection Efficiency

The absolute detection efficiency was estimated from the measured values of position dependent efficiency, energy dependent efficiency, charge state fraction and the angle dependent efficiency along with some theoretical estimates as mentioned in the last chapter. The energy, angular and charge state distribution were measured at one energy for all the systems studies and were compared with the theoretical

predictions. The experimental charge state distribution was compared with the predictions of the Sayers semi-empirical formula. According to Sayers semi-empirical formalism [1], the distribution of the charge state is given by

$$F(q) = \frac{1}{\rho\sqrt{2\pi}} exp\left[\frac{-t^2}{2(1+\epsilon t)}\right] \tag{6.1}$$

where,

$$\begin{aligned} t^2 &= \frac{q - q_o}{\rho} \\ \frac{\epsilon}{\rho} &= 0.007Z - 0.7\frac{v}{c} \\ \rho &= 0.48Z^{0.45}\left[\frac{q_o}{Z}(1 - \frac{q_o}{Z})\right] \\ \frac{q_o}{Z} &= 1 - 1.03exp\left[-47.3Z^{-0.380}(\frac{v}{c})^{0.860}\right] \end{aligned} \tag{6.2}$$

Here q_o is the mean charge state and Z is the atomic number. There was good agreement between the Sayers predictions and the experimental distributions obtained as can be seen in Figs. 6.1, 6.3.

The angular distribution and energy distribution were compared with the predictions of the code PACE2. The PACE2 is a Monte-Carlo code which can be used as a good tool for the estimation of evaporation cross section, angular distribution etc. To get the energy and angular distributions PACE2 calculations have been done with 10000 events for a particular energy of a particular reaction. In the calculations, the PACE2 energy spectrum was convoluted with a bin size considering the mean evaporation residue energy and the energy loss in the target. The convoluted yields for each particles (having same Z and A) were multiplied by the Gaussian obtained from a fit to the measured energy distribution of the RMS using α-source (Fig. 5.6). This will give the number of particles reaching the focal plane of HIRA considering the energy acceptance. The ratio of particle transmitted through HIRA to the number of particles entering in HIRA will give the energy dependent efficiency. The angular part of efficiency was obtained as the ratio of number of particles entering in HIRA (limited by the opening) to the number of particles produced in the 4π angle.

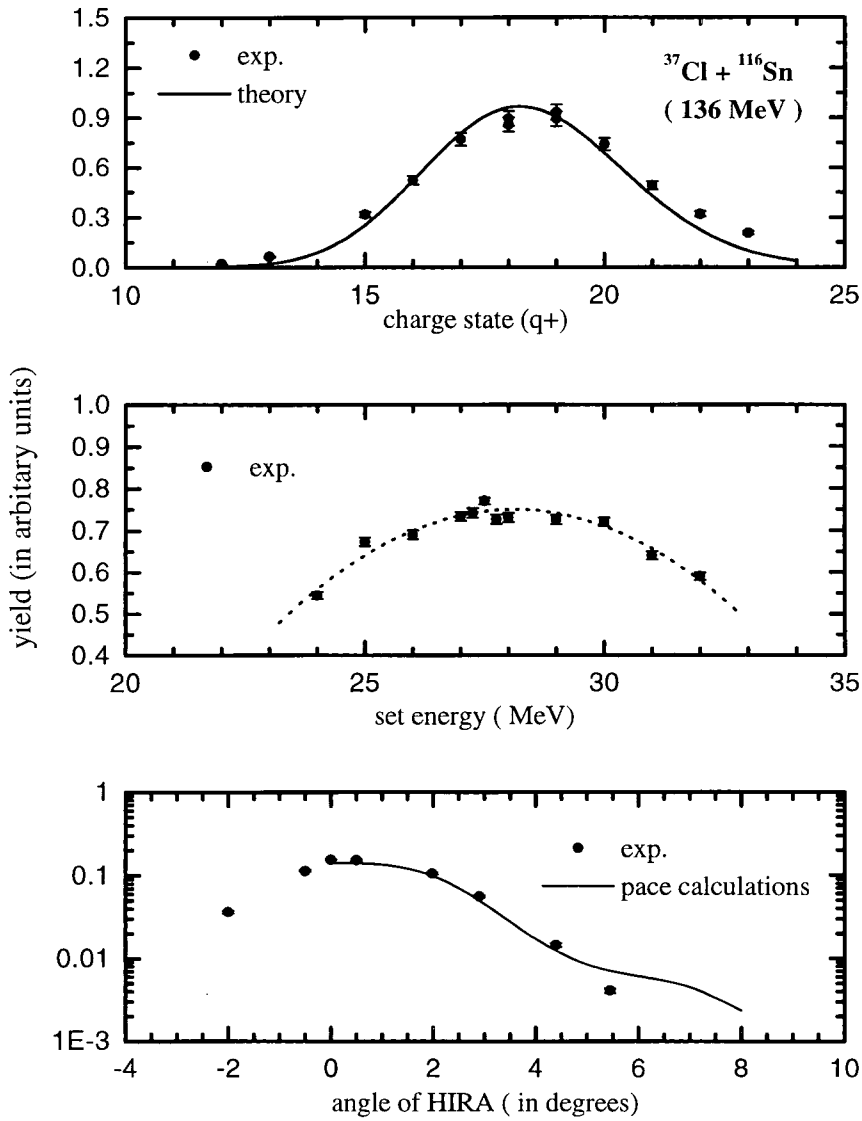

Figure 6.1: The measured charge state distribution, energy distribution and angular distribution for the system ^{37}Cl + ^{116}Sn at a beam energy of 136 MeV.

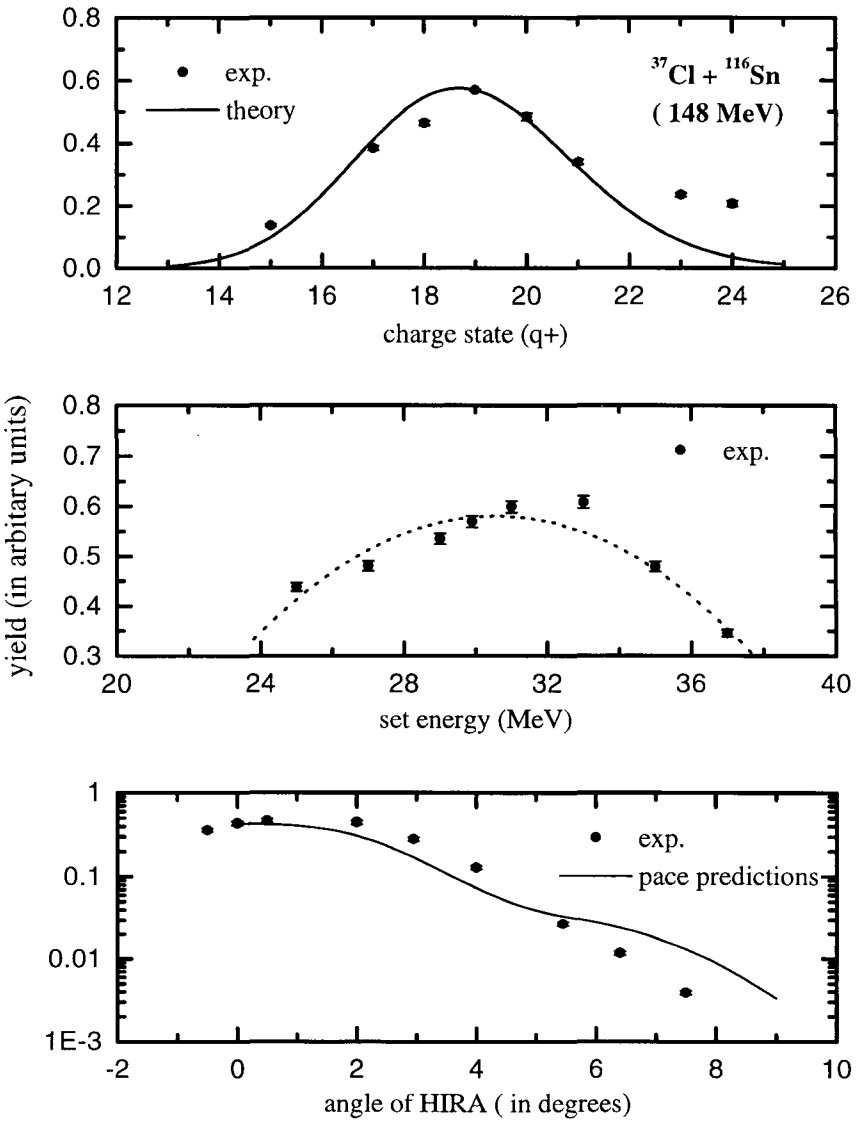

Figure 6.2: The measured charge state distribution, energy distribution and angular distribution for the system ^{37}Cl + ^{116}Sn at a beam energy of 148 MeV.

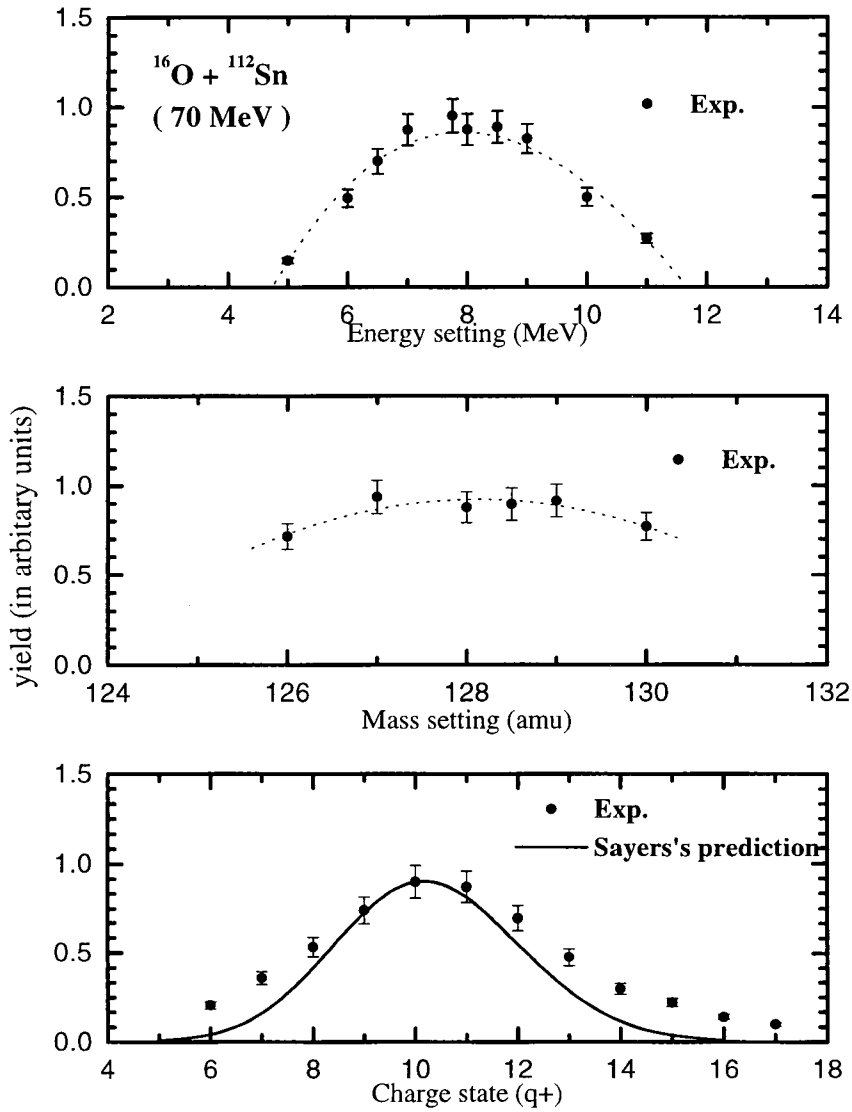

Figure 6.3: The measured charge state distribution, energy distribution and mass distribution for the system $^{16}O + ^{112}Sn$ at a beam energy of 70 MeV.

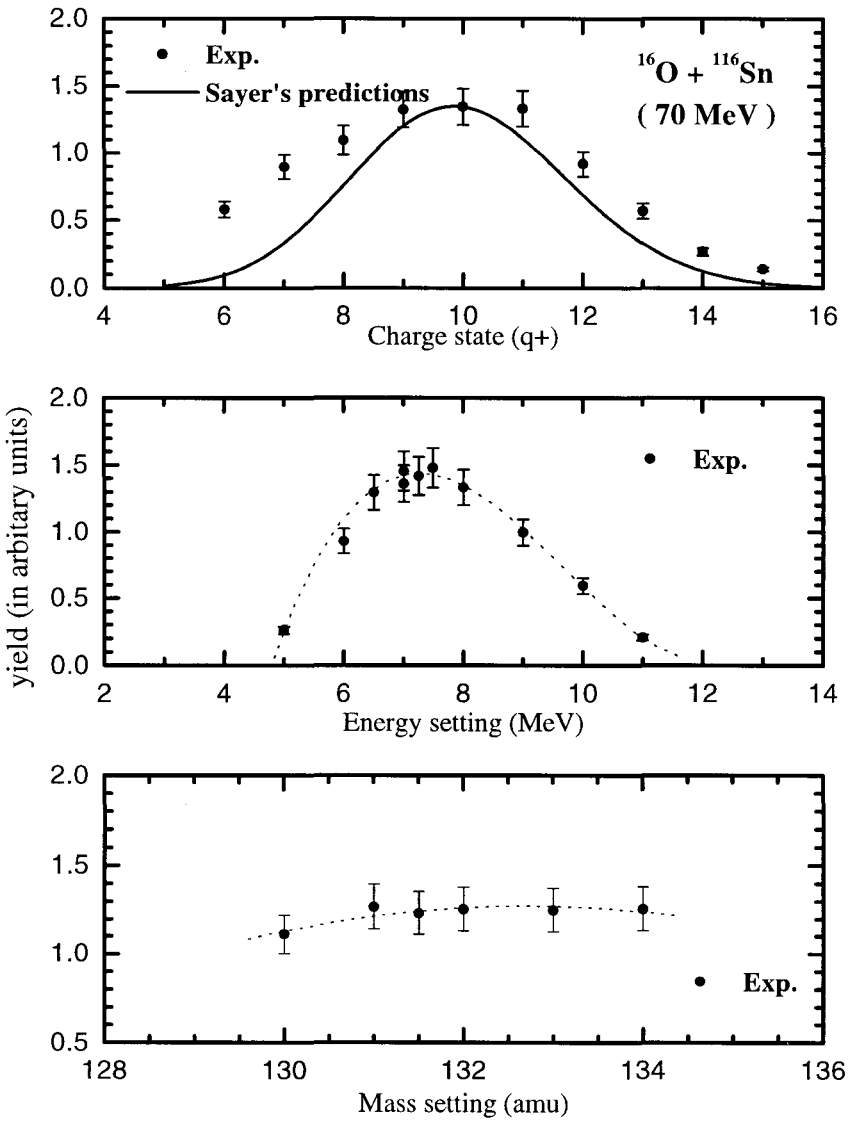

Figure 6.4: The measured charge state distribution, energy distribution and mass distribution for the system $^{16}O + ^{116}Sn$ at a beam energy of 70 MeV.

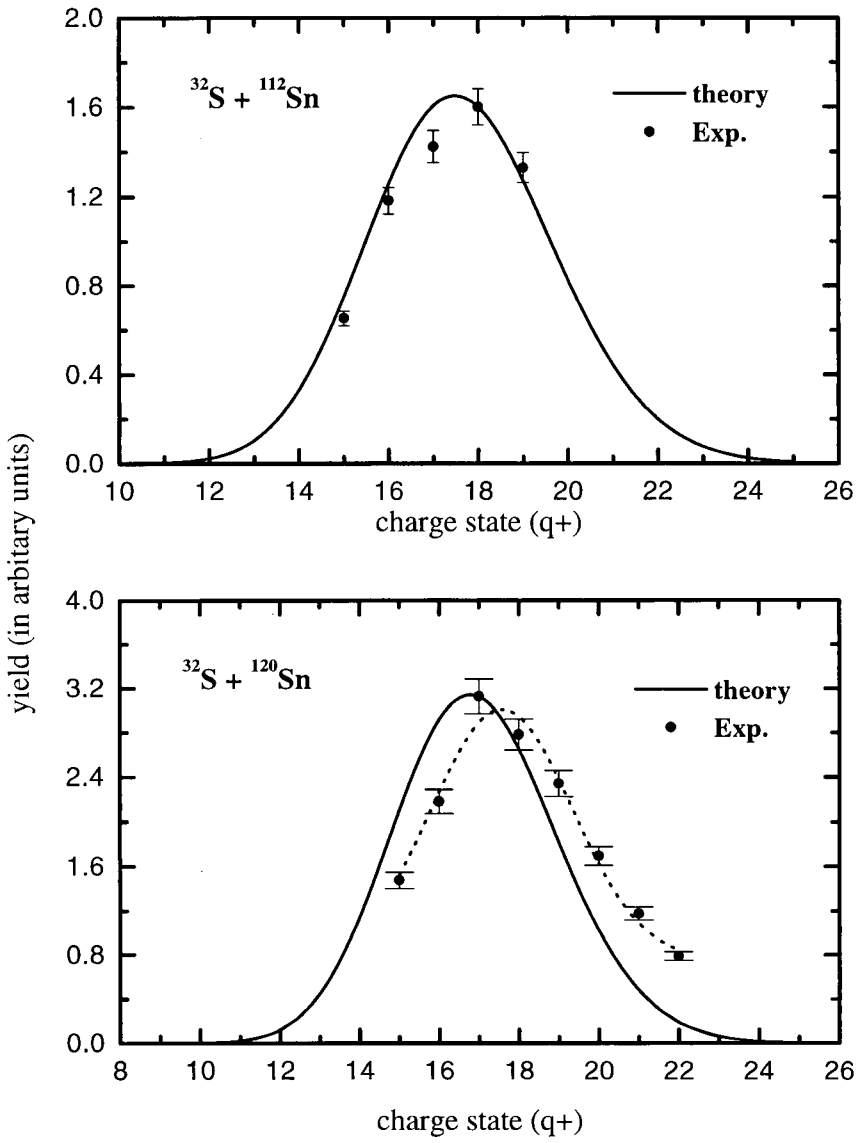

Figure 6.5: The measured charge state distribution and the theoretical predictions for the system ^{32}S + ^{112,120}Sn at a beam energy of 140 MeV.

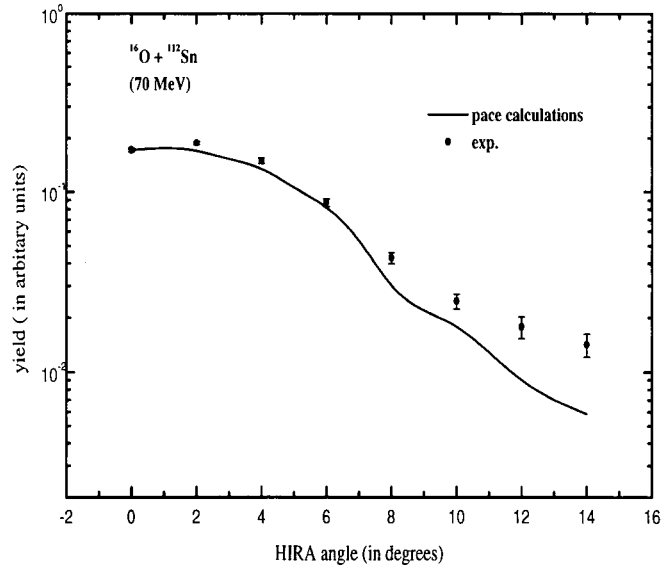

Figure 6.6: The measured angular distribution and the PACE2 predictions for the system $^{16}O + ^{112}Sn$ at a beam energy of 70 MeV.

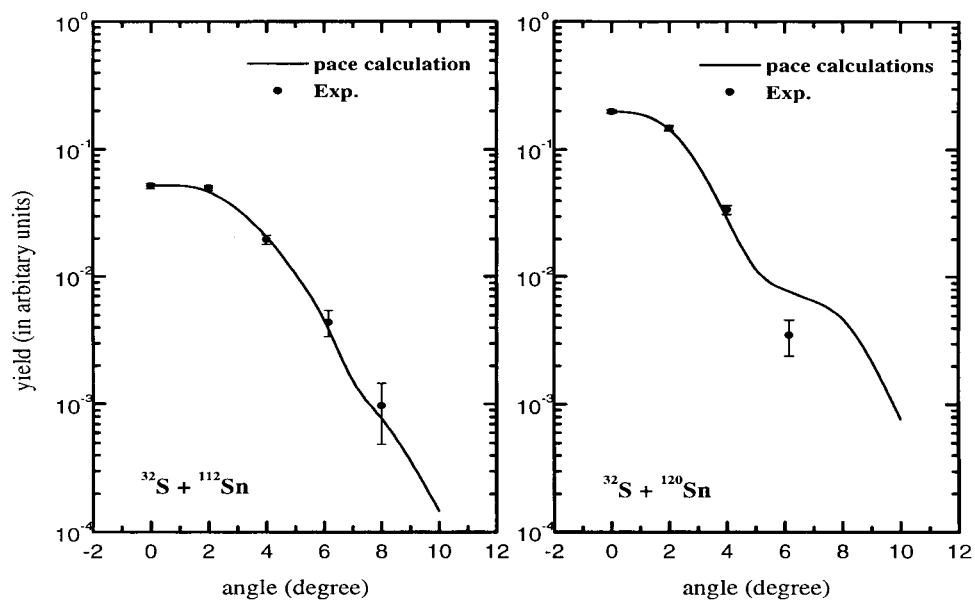

Figure 6.7: The measured angular distribution and the PACE2 predictions for the system $^{32}S + ^{112,120}Sn$ at a beam energy of 140 MeV.

The measured energy and angular distribution were found to be in good agreement with the PACE2 estimates (Figs. 6.6, 6.7).

Since the measured and the calculated distributions agreed well at one energy for each system so it was assumed that the same will be true for all energies. The energy and angular distribution obtained from PACE2 calculations were used to calculate the energy dependent efficiency and angle dependent efficiency for all energies. The charge state fraction was obtained from the Sayers formula. The estimated total efficiency at a particular energy can be written as

$$\eta_{total}(E,\theta,Z,A) = \eta_E(E,Z,A) \times \eta_\theta(E,Z,A,\theta) \times f_{q^+}(E,Z,A) \tag{6.3}$$

with

$$\eta_E(E,Z,A) = \frac{N(E)T(E)}{N(E)_t} \tag{6.4}$$

where $N(E)$ is the number of particles produced in each energy bin, $T(E)$ the transmittance of HIRA for the particle with energy E and $N(E)_t$ is the total number of particles produced. The $\eta_\theta(E,Z,A)$ is given by

$$\eta_\theta(E,Z,A,\theta) = \frac{N_H}{N(\theta)} \tag{6.5}$$

where N_H is the number of particles entering HIRA through the solid angle defining aperture (SADA), which can be kept at 1 msr, 5 msr or 10 msr and N(θ) is the number of particles produced in all angles. The quantity $f_{q^+}(E,Z,A)$ represents the probability of the charge state, q^+ for the particular nuclei. It was found that the efficiency varied smoothly over the energy range studied. This estimated efficiency as a function of energy was used in the calculation of the fusion cross section.

6.1.1 Estimation of the Fusion Cross Section

In the estimation of fusion cross section, the evaporation residue cross section was taken to be equal to the total fusion cross section since the fission contribution is negligible in this energy range for the systems studied. The measured cross-section

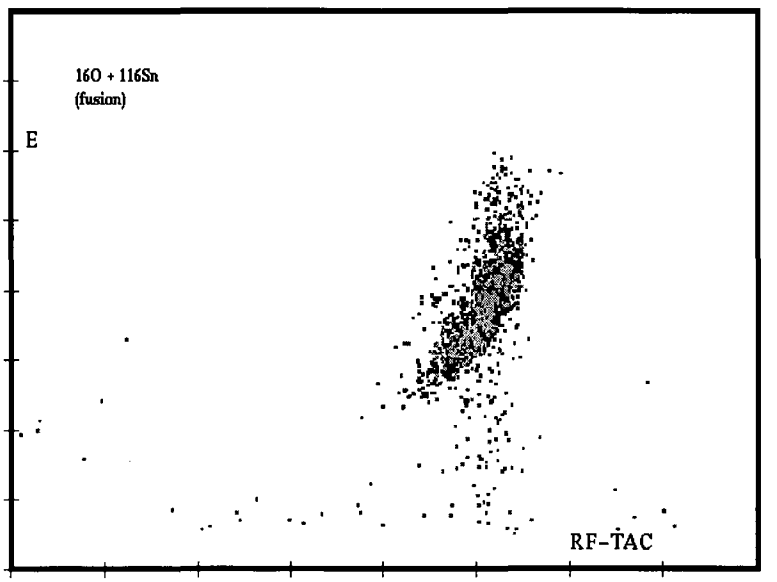

Figure 6.8: A typical two dimensional plot of TOF vs Energy. A clear separation of the ER's from the background can be seen.

forms a part of the total residue cross-section which has been calculated using the expression

$$\sigma_{fus} = \frac{1}{\epsilon}\left(\frac{Y_{ER}}{Y_M}\right)\left(\frac{d\sigma}{d\Omega}\right)_R \Omega_M \qquad (6.6)$$

where ϵ is the estimated HIRA efficiency, Y_{ER} is the yield of the evaporation residues (ER's), Y_M is the monitor counts, $(d\sigma/d\Omega)_R$ is the Rutherford cross section in the laboratory system and Ω_M is the solid angle subtended by the monitor detector. The ER yield was taken from the two dimensional plots of energy *vs* time of flight where they were clearly separated from the beam background. A typical two dimensional spectrum is shown in Fig. 6.8. Yield for different evaporation channels was not extracted but the total ER counts were taken. For the monitor counts the geometric mean of the counts in the four monitors was taken. The experimental errors include the statistical error and the systematic errors. The major source of systematic error comes from the uncertainty in the estimated HIRA efficiency.

Correction for Energy Loss in the Target

The beam energy was calculated directly from the field of the analyser magnet of the Pelletron which has been measured through a NMR probe. Correction has been made for the energy loss of the beam in the target. The correction made was equal to energy loss in half the thickness of the target. This corrected energy was used in the further calculations. Care was also taken of the energy loss of the recoils through half thickness of the target.

6.1.2 Calculation of Barrier Distribution

Barrier distribution has been extracted from the fusion excitation function by taking the second derivative of the product of the centre of mass energy E and σ_{fus} with respect to energy [2]. The second derivative was calculated using a point difference method as given below. The barrier distribution is defined at energy $(E_1 + 2E_2 + E_3)/4$ as

$$\frac{d^2(E\sigma_{fus})}{dE^2} = 2\left(\frac{(E\sigma_{fus})_3 - (E\sigma_{fus})_2}{E_3 - E_2} - \frac{(E\sigma_{fus})_2 - (E\sigma_{fus})_1}{E_2 - E_1}\right)\left(\frac{1}{E_3 - E_1}\right) \quad (6.7)$$

where $(E\sigma_{fus})_i$ are evaluated at energies E_i. For the case of equal energy increments $\Delta E = (E_2 - E_1) = (E_3 - E_2)$ the above expression becomes

$$\frac{d^2(E\sigma_{fus})}{dE^2} = \left(\frac{(E\sigma_{fus})_3 - 2(E\sigma_{fus})_2 + (E\sigma_{fus})_1}{\Delta E^2}\right) \quad (6.8)$$

The statistical error δ_c associated with the second derivative at energy E is given by

$$\delta_c = \left(\frac{E}{\Delta E^2}\right)\left[(\delta\sigma_{fus})_1^2 + 4(\delta\sigma_{fus})_2^2 + (\delta\sigma_{fus})_3^2\right]^{1/2} \quad (6.9)$$

where $(\delta\sigma_{fus})_i$ are the absolute errors in the cross sections.

In our measurement since the energy steps were not exactly equal we have used the eqn no. 6.7 for calculating the second derivative. A ΔE of nearly 1.75 - 2.25 MeV in the centre of mass frame was used.

6.1.3 Results

The fusion excitation function and the barrier distribution were calculated for all the systems studied as outlined in the previous section. The results are summarised in the following sections.

^{37}Cl + ^{116}Sn System.

The measured charge state, energy and angular distribution at two energies 136 and 148 MeV are shown in Fig. 6.1 and Fig. 6.2 respectively. The efficiency was extracted as a function of energy as described in the previous section and used in the calculation of the fusion cross section. The calculated fusion excitation function is shown in Fig. 6.9. The second derivative was extracted using the point difference formula with $\Delta E \approx 2$ MeV and is shown in Fig. 6.10. The excitation function and the barrier distribution are compared with the predictions of the 1D-BPM and we can see clear departures from the model predictions. As can be seen from Fig. 6.9 the excitation function is not very smooth giving large scatter in the second derivative specially at high energies. Also the lowest cross section measured in this case is roughly 2 mb, so the low energy part of the barrier distribution could not be extracted.

^{16}O + ^{112,116}Sn Systems.

The charge state, mass and energy distributions for the two systems ^{16}O + ^{112,116}Sn are shown in Fig. 6.3 and Fig. 6.4 respectively. The angular distribution was measured only for the ^{112}Sn system and is shown in Fig. 6.6. From these measured quantities the efficiency was extracted as explained before and the fusion cross sections were calculated. The fusion excitation functions for the two systems are shown in Fig. 6.11 and Fig. 6.12 along with the predictions of the 1D-BPM. An asymptotic barrier shift of about 1 MeV can be seen. The extracted barrier distributions for the two systems which are very well defined with a prominent peak at a lower energy

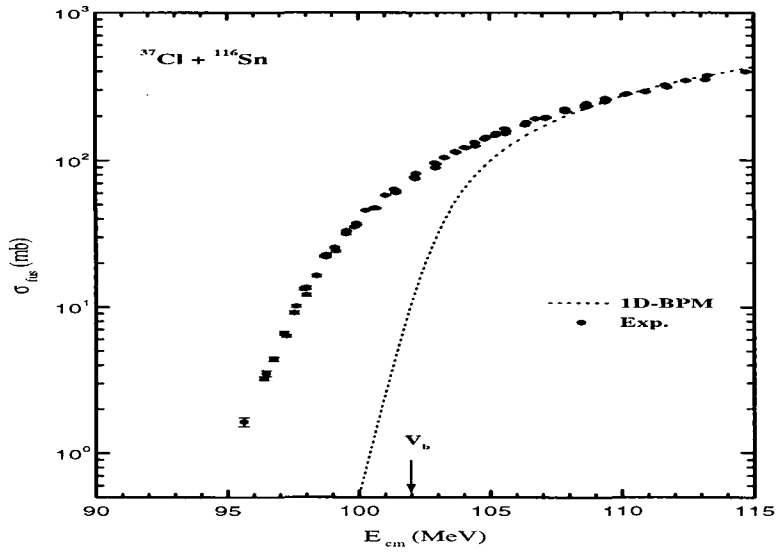

Figure 6.9: The measured excitation function for the system ^{37}Cl + ^{116}Sn. Also shown in the figure is the prediction of the one dimensional barrier penetration model (1D-BPM).

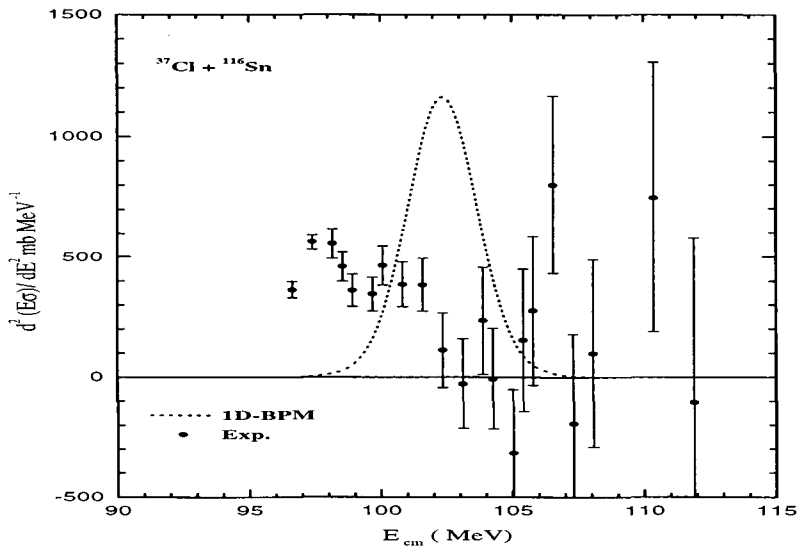

Figure 6.10: The barrier distribution extracted from the fusion excitation function for the system ^{37}Cl + ^{116}Sn shown along with uncoupled barrier as predicted by the 1D-BPM.

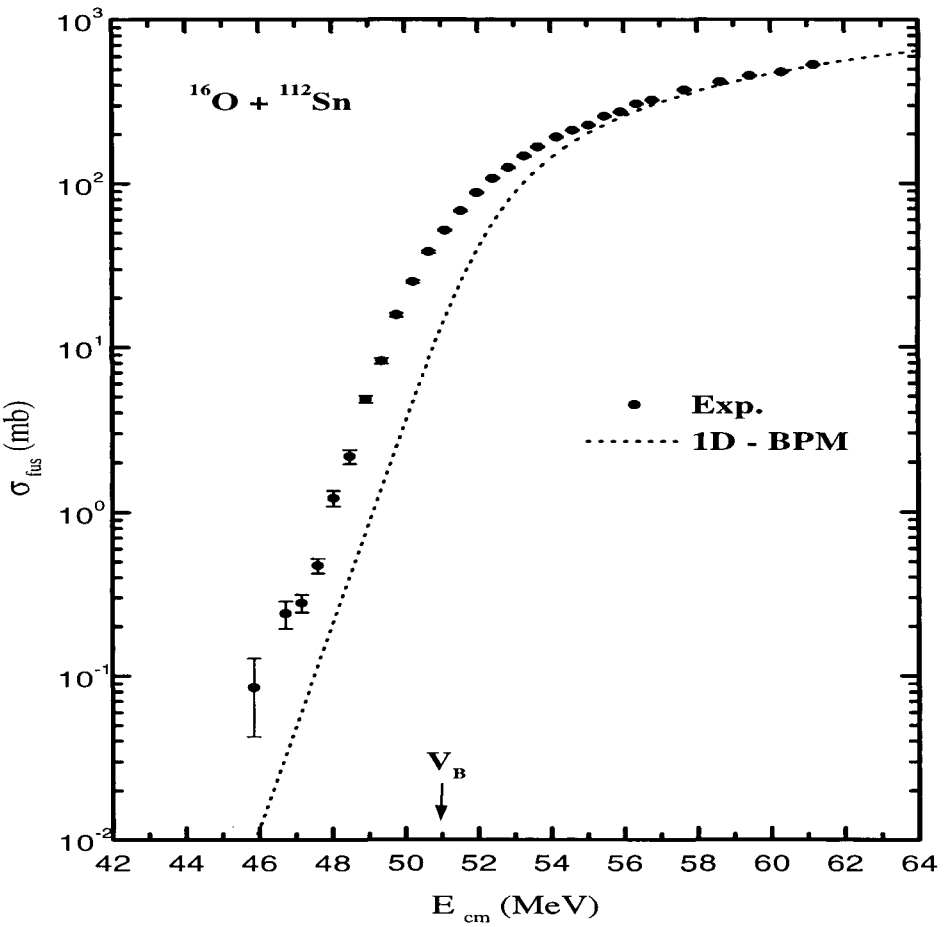

Figure 6.11: The measured fusion excitation function for the system ^{16}O + ^{112}Sn shown along with the predictions of the 1D-BPM.

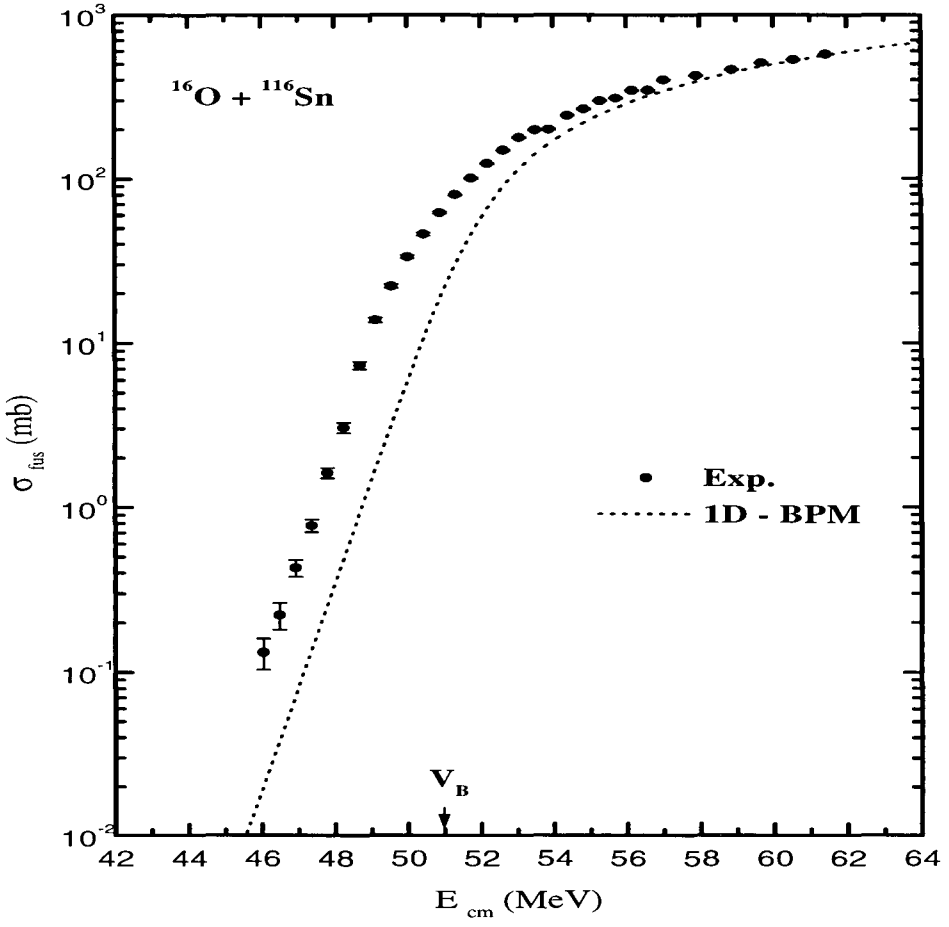

Figure 6.12: The measured fusion excitation function for the system $^{16}O + ^{116}Sn$ shown along with predictions of the 1D-BPM.

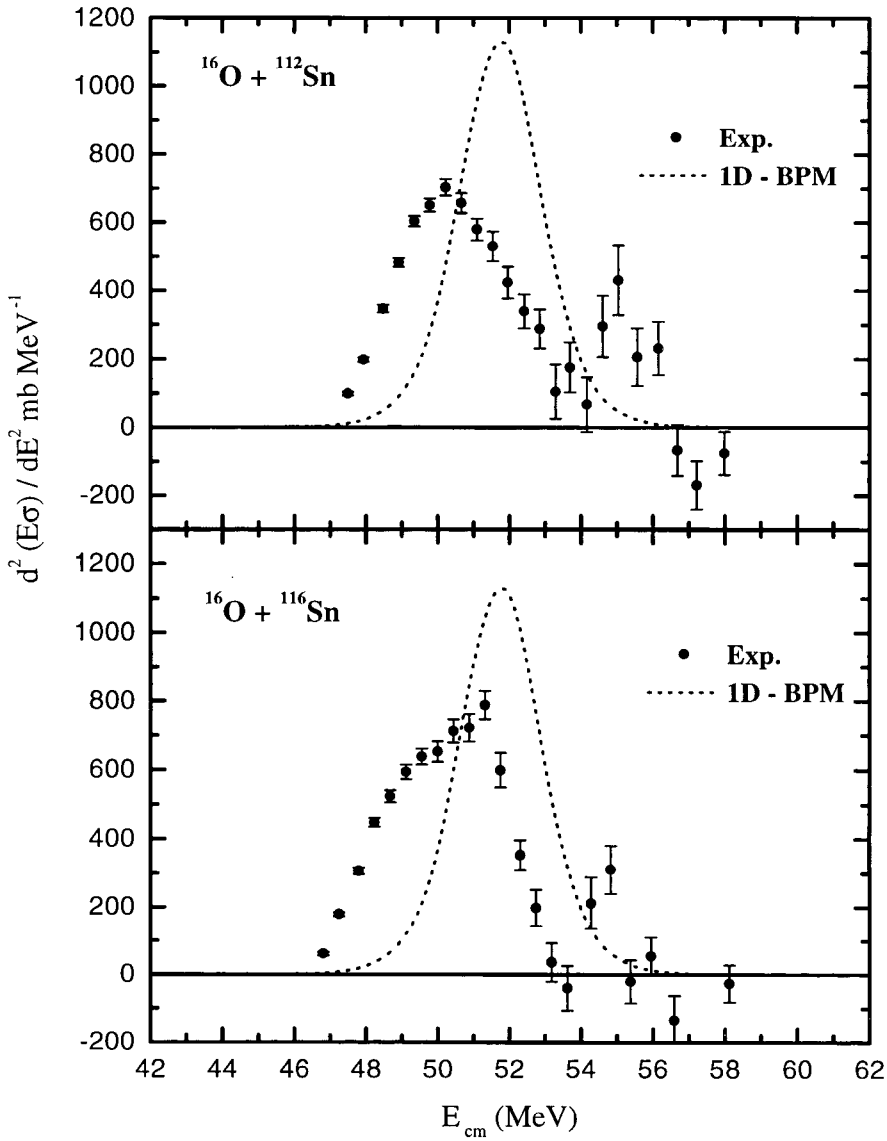

Figure 6.13: The second derivative as extracted from the fusion excitation function for the systems $^{16}O + ^{112,116}Sn$ shown along with predictions of the 1D-BPM.

than the uncoupled barrier are shown in Fig. 6.13.

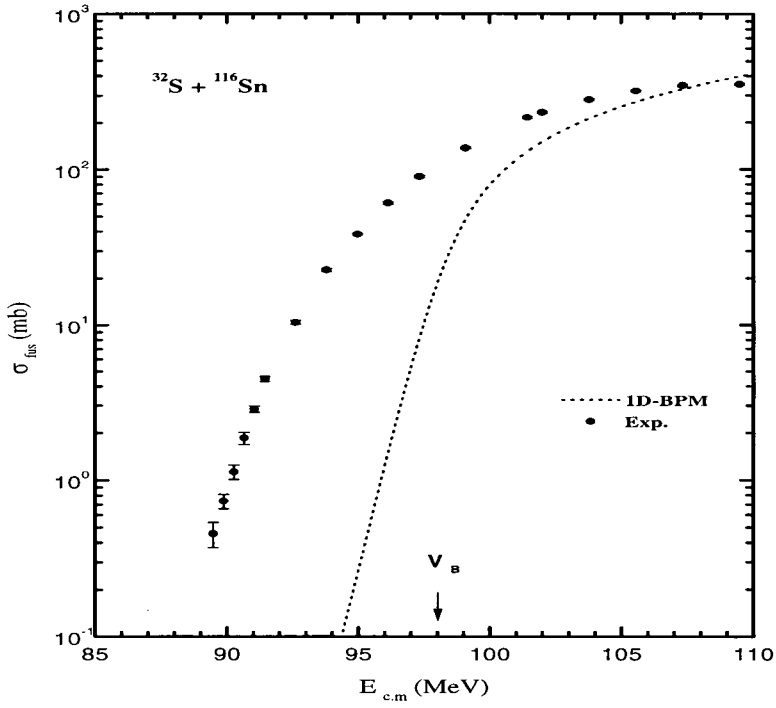

Figure 6.14: The measured fusion excitation function for the system $^{32}S + ^{116}Sn$ shown along with the predictions of the 1D-BPM.

$^{32}S + ^{112,116,120}Sn$ Systems.

The charge state, energy and angular distributions were measured for these systems and representative plots are shown in Fig. 6.5 and Fig. 6.7. The fusion excitation functions for the systems $^{32}S + ^{116}Sn$, $^{32}S + ^{112}Sn$ and $^{32}S + ^{120}Sn$ are shown in Fig. 6.14, Fig. 6.14 and Fig. 6.16 respectively. The barrier distribution was extracted only for the ^{112}Sn and ^{120}Sn case and is shown in Fig. 6.17. As observed for the other systems, we see clearly that the 1D-BPM fails to explain the experimental data.

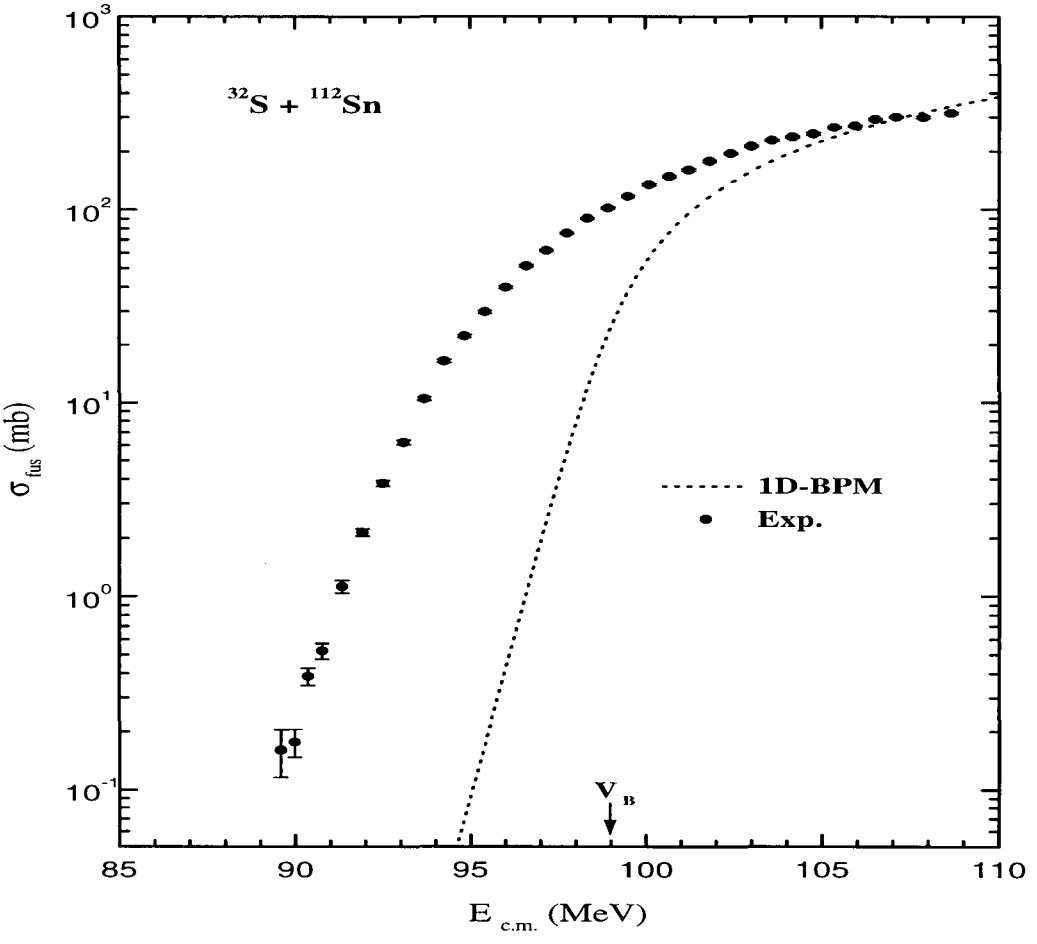

Figure 6.15: The measured fusion excitation function for the system ^{32}S + ^{112}Sn shown along with the predictions of the 1D-BPM.

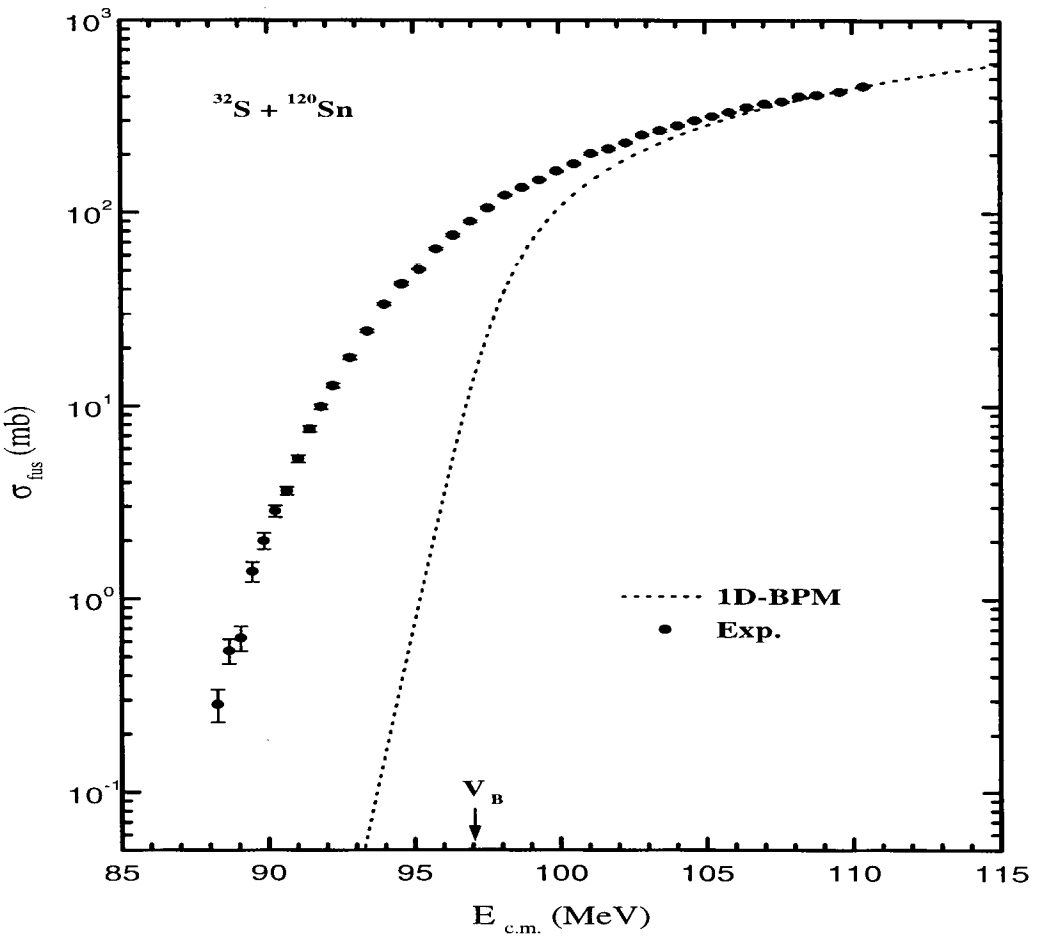

Figure 6.16: The measured fusion excitation function for the system ^{32}S + ^{120}Sn shown along with the predictions of the 1D-BPM.

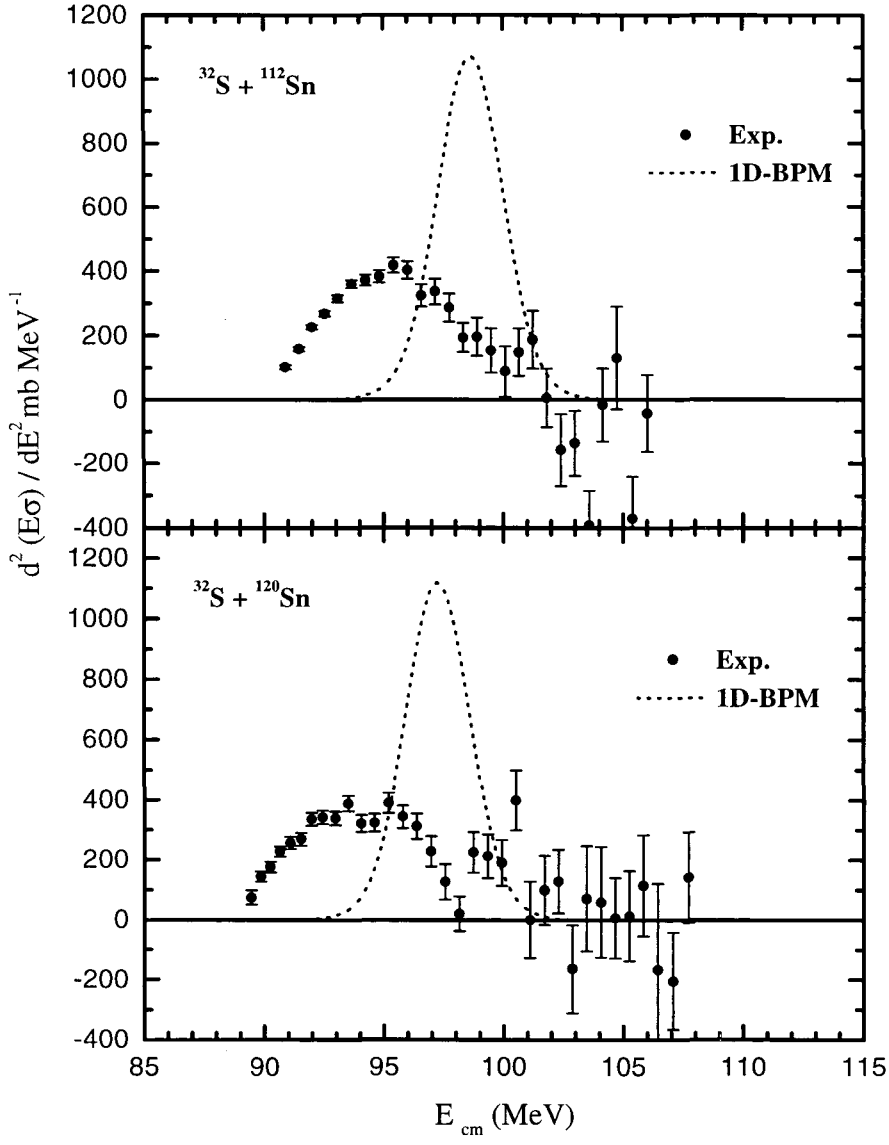

Figure 6.17: The fusion barrier distribution extracted from the fusion excitation function for the systems ^{32}S + ^{112,120}Sn shown along with the uncoupled barrier.

6.2 Quasi-Elastic Scattering

The recoiling Sn-like particles were detected at the focal plane of HIRA, after filtering out the beam. These particles give the quasi-elastic yield which includes all elastic and inelastic scattering yield. These events of interest were cleanly identified in the two dimensional plot of energy *vs* time of flight. The detector resolution did not allow the separation of the elastic and inelastic events, however transfer products were separated and were not included in calculating the quasi-elastic cross sections.

6.2.1 Estimation of the Differential Cross Section

From the measured quasi-elastic yield the differential scattering cross section was calculated as

$$d\sigma_{qel}(\theta) = \frac{Y_{qel}(\theta)}{Y_R(\theta_M)}\sigma_R(\theta_M)\frac{\Omega_M}{\Omega} \tag{6.10}$$

where $Y_{qel}(\theta)$ is the yield of the quasi-elastic events detected in the solid angle Ω, $Y_R(\theta_M)$ is the rate of Rutherford scattering detected by a monitor detector at θ_M subtending a solid angle Ω_M and $\sigma_R(\theta_M)$ is the Rutherford scattering cross section. In our measurement the angle $\theta = 180°$ so the differential quasi-elastic cross section has been normalised to the Rutherford differential cross section at $\theta = 180°$, $d\sigma_R$ so that the data points at the lowest energies equal unity. The ratio $d\sigma_{qel}/d\sigma_R$ is nothing but the reflection coefficient if $\theta = 180°$ *i.e.*,

$$R(E) = \frac{d\sigma_{qel}}{d\sigma_R}|_{\theta=180} \tag{6.11}$$

6.2.2 Calculation of Barrier Distribution

The barrier distribution from quasi-elastic data is given by the first derivative of R(E), the reflection coefficient with respect to energy [3];

$$\begin{aligned} D^{qel}(E) &= -\frac{dR(E)}{dE} \\ &= -\frac{d}{dE}\left[\frac{d\sigma_{qel}}{d\sigma_R}(E, \theta = 180°)\right] \end{aligned} \tag{6.12}$$

The differentiation is performed for alternate points, at energy E_2 the value is given by

$$\frac{d}{dE}\left(\frac{d\sigma_{qel}}{d\sigma_R}\right)_{E_2} = \frac{(\frac{d\sigma_{qel}}{d\sigma_R})_{E_1} - (\frac{d\sigma_{qel}}{d\sigma_R})_{E_3}}{E_1 - E_3} \tag{6.13}$$

and the associated statistical error is given by

$$\delta_e = \frac{1}{\Delta E}\left[\delta_1^2 + \delta_3^2\right]^{\frac{1}{2}} \tag{6.14}$$

where $\Delta E = E_1 - E_3$ and δ_i are the absolute uncertainties in the ratio of the quasi-elastic to Rutherford differential cross section. The energy step that we have used in the calculation is around 2 MeV in the centre of mass.

6.2.3 Results

The barrier distribution was extracted from the measured excitation functions as discussed in the previous sections for the systems ^{16}O + ^{120}Sn and ^{32}S + ^{120}Sn. The results are summarised below and the important qualitative features of this representation of the barrier distribution are also discussed.

^{16}O + ^{120}Sn System

The quasi-elastic scattering excitation function along with the calculated barrier distribution is shown in Fig. 6.18. A $\Delta E = 2$ MeV was used in the calculation of the first derivative that is the barrier distribution.

^{32}S + ^{120}Sn System

Fig. 6.19 displays the excitation function and the barrier distribution for this system. In this case a $\Delta E = 4$ MeV was used in the calculation of the barrier distribution.

The qualitative features of the barrier distribution extracted from back-angle scattering excitation function can be inferred from observing the Figs. 6.18 and 6.19. It can be seen that the excitation functions fall monotonically with energy and

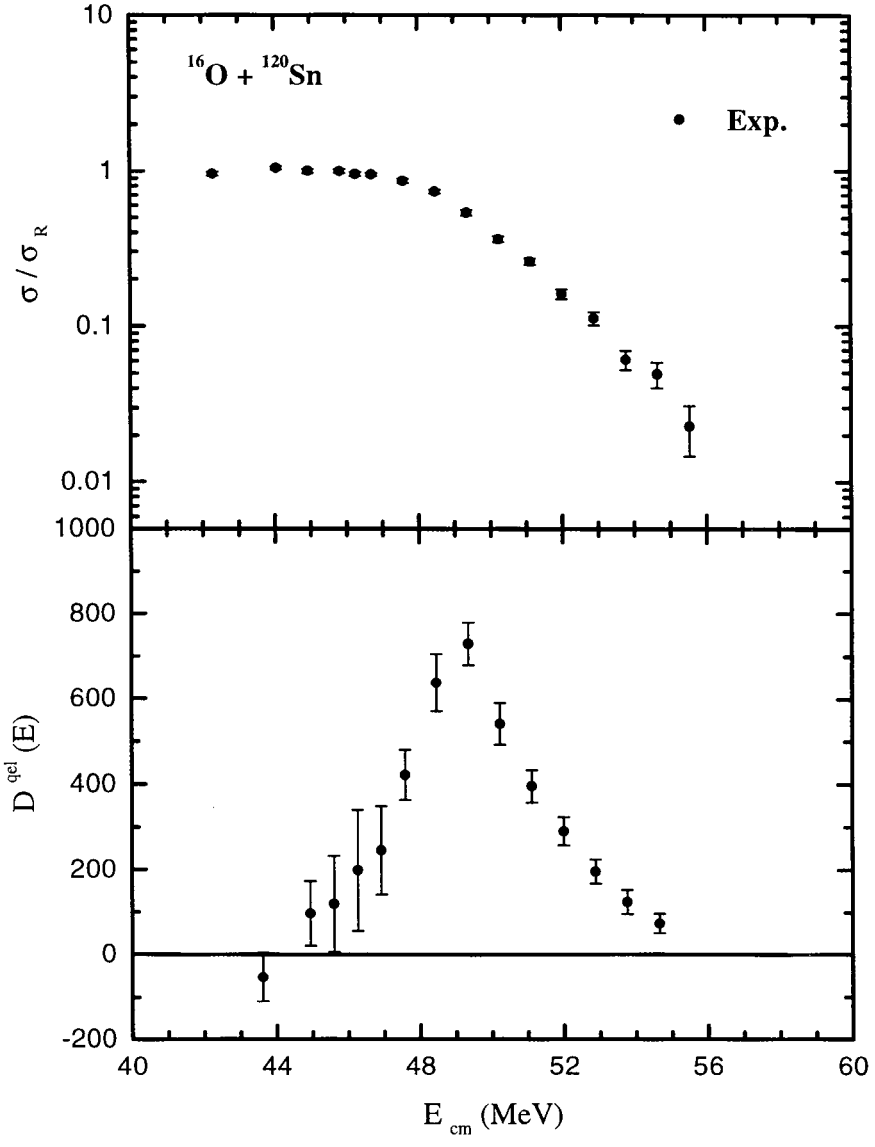

Figure 6.18: The measured quasi-elastic excitation function for the system ^{16}O + ^{120}Sn shown along with the extracted barrier distribution.

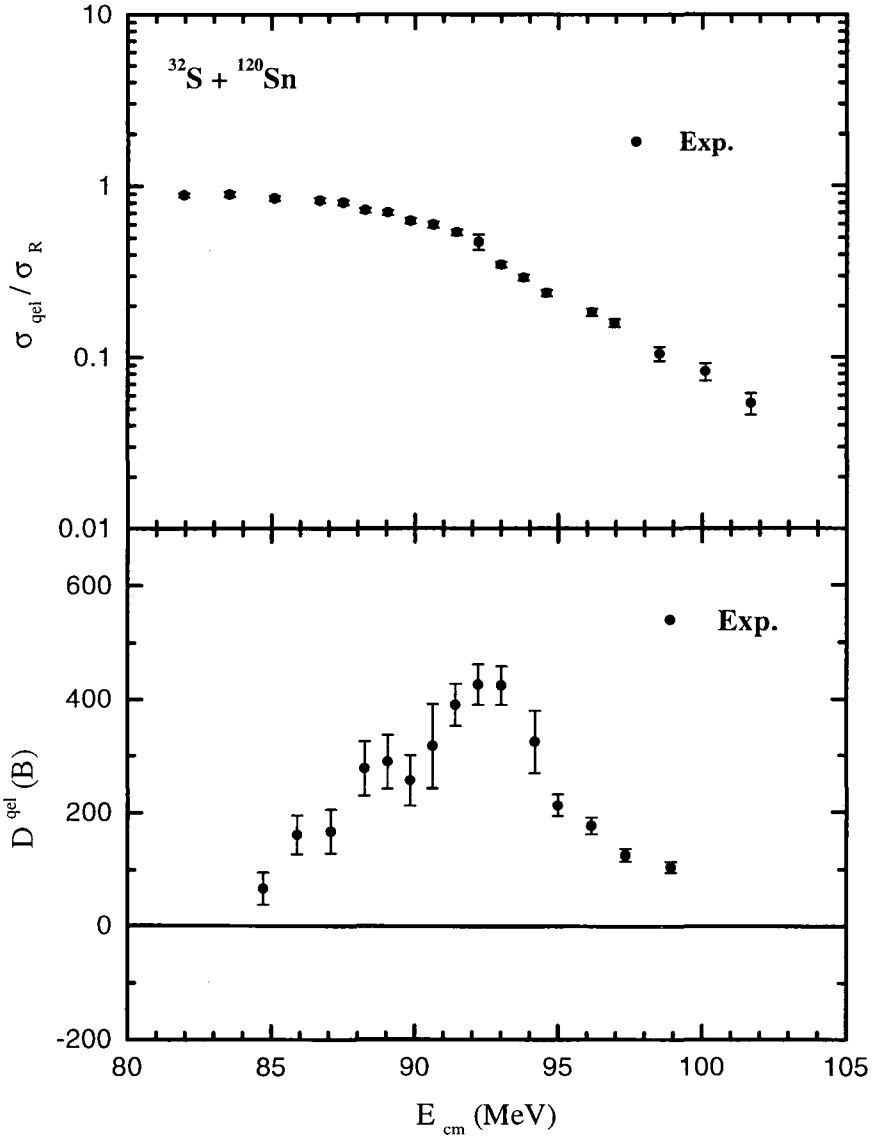

Figure 6.19: The measured quasi-elastic excitation function for the system ^{32}S + ^{120}Sn shown along with the extracted barrier distribution.

the rate of decrease is different for the two cases. The O + Sn excitation function falls more rapidly than the other resulting in a narrower barrier distribution for that case. Looking at the barrier distributions it can be said that they have less scatter in comparison to the second derivative of the fusion excitation function (see Figs. 6.13, 6.17). The difference is very pronounced at above barrier energies where there are no negative values in this case. However, at the low energy end, it is the fusion data which is better defined. Also the width of the peaks in $D^{qel}(E)$ is larger than $D^{f}(E)$ making this representation less sensitive to the barrier structure (compare Figs. 6.13 and 6.18).

Another significant feature of the representation $D^{qel}(E)$ is that it falls off smoothly at higher energies. This featureless, smooth tail of $D^{qel}(E)$ at higher energies has been a common feature of all earlier measurements [3, 4] and it persisted even in heavier systems. It was suggested that this tail is due to the de-phasing of the scattering amplitudes and not due to diffraction effects in which case it should have been absent in the heavier systems. In our measurements we do not see any sign of oscillations in the barrier distribution. For the systems $^{16}O + ^{154}Sm$, ^{186}W studied by Timmers [3, 4] at a laboratory angle of 170° there was an oscillatory behaviour observed at the lower energies. This is an indication to the point that extreme back angle measurements are essential to avoid the oscillatory behaviour which is associated with diffraction effects in scattering.

Thus we have successfully measured the quasi-elastic cross sections at 180° and extracted the barrier distribution. The barrier structure below the uncoupled barrier is reflected in this distribution though the resolution is much poorer than that of $D^{f}(E)$. At higher energies, the distribution tails off smoothly. So the representation $D^{qel}(E)$ may be useful in the determination of the barrier distribution for systems which have pronounced barrier structures below the uncoupled barrier. This information may be complimentary to that obtained from the barrier distribution representation of the fusion data.

Bibliography

[1] R. O. Sayer, Revue de physique appliquëe **12**, 1543 (1972).

[2] N. Rowley, G. R.Satchler, and P. H. Stelson, Phys. Lett. **B254**, 25 (1991).

[3] H. Timmers, J. R. Leigh, M. Dasgupta, D. J. Hinde, R. C. Lemmon, J. C. Mein, C. R. Morton, J. O. Newton, N. Rowley, Nucl. Phys. **A584**, 190 (1994).

[4] H. Timmers, Ph.D. Thesis submitted to the Australian National University, 1996.